Available online at www.sciencedirect.com
SCIENCE DIRECT®
Journal of Catalysis 224 (2004) 429–440
JOURNAL OF CATALYSIS
www.elsevier.com/locate/jcat

N_2O decomposition over iron-containing zeolites prepared by different methods: a comparison of the reaction mechanism

Gerhard D. Pirngruber,[a,*] Marco Luechinger,[a] Pijus K. Roy,[a] Andrea Cecchetto,[a] and Panagiotis Smirniotis [b]

[a] *Institute for Chemical and Bioengineering, Swiss Federal Institute of Technology (ETH) Zurich, Wolfgang-Pauli-Str. 10, CH-8093 Zurich, Switzerland*
[b] *Chemical & Materials Engineering Department, University of Cincinnati, Cincinnati, OH 45221-0012, USA*

Received 18 December 2003; revised 19 March 2004; accepted 22 March 2004

Available online 17 April 2004

Abstract

Iron-containing zeolites were prepared by aqueous ion exchange, sublimation of $FeCl_3$, or hydrothermal synthesis and were modified by steaming at 873 K. The samples contained different kinds of iron species ranging from isolated iron atoms to small clusters that contain a few atoms and somewhat larger oligomers. Yet, the dynamic behavior of all samples in N_2O decomposition was qualitatively similar. Pulse experiments showed that a slow and fast pathway of O_2 formation, which is the rate-limiting step of the reaction, exists. Both contributed to the overall activity. The fast pathway dominated on isolated iron sites, whereas the contribution of the slow pathway increased on catalysts with high iron loadings. Steaming led to an agglomeration of the iron clusters and increased the activity (with one exception). The steamed samples had a peculiar time-on-stream behavior. They exhibited a very high initial activity and then slowly decayed to steady state. This indicates that steaming did not merely agglomerate the iron clusters, but qualitatively changed the nature of the active sites.

Keywords: N_2O decomposition; Iron zeolite; Fe-ZSM-5; Fe-ZSM-12; Steaming; Pulse response; Step response; UV-Vis; EXAFS

1. Introduction

Iron zeolites have attracted much attention as catalysts for the abatement of N_2O emissions in nitric and adipic acid plants. They are insensitive to the presence of other components in the exhaust stream, like O_2, NO, SO_2, and H_2O [1,2]. Other metal-based catalysts are more active for N_2O decomposition, but cannot maintain this high activity in a real exhaust gas mixture [3–11]. Also in the selective catalytic reduction of NO_x with NH_3 [12–15] or hydrocarbons [16–18], iron zeolites were reported to be active and stable catalysts.

Iron zeolites can be prepared by several methods. The most common one is to introduce iron by postsynthetic ion exchange with an aqueous solution of an iron salt. A difficulty in the aqueous ion exchange is that Fe^{3+} ions tend to agglomerate and precipitate. Only over a very narrow pH range they are stable as positively charged ions, which can react with the ion-exchange sites of the zeolite. Fe^{2+} ions, on the other hand, are easily oxidized to Fe^{3+} [19,20]. Therefore, chemical vapor deposition of $FeCl_3$ onto the zeolite was suggested as an alternative method to introduce iron in high loadings [21]. The method is very reproducible and leads to a ratio of one Fe atom per Brønsted acid site. It is also possible to incorporate iron into the zeolite framework already during the synthesis of the zeolite. In a framework position iron is not catalytically active [2,22]. It has to be extracted from the framework by steaming at high temperatures. These materials showed very high turnover frequencies in N_2O decomposition [2] and a high stability toward SO_2 [1].

To date it has not been satisfactorily shown whether the different preparation methods lead to similar types of active iron sites or whether there are fundamental differences in the properties of the iron zeolites depending on their method of preparation. For the materials prepared by hydrothermal synthesis followed by steaming the formation of a very active oxygen species, called α-oxygen was claimed [23–25]. It can, therefore, be expected that these catalysts behave differently from those prepared by postsynthetic ion exchange.

* Corresponding author. Fax: +41 1 632 1162.
E-mail address: pirngruber@chem.ethz.ch (G.D. Pirngruber).

0021-9517/$ – see front matter
doi:10.1016/j.jcat.2004.03.031

In this paper we present a detailed comparison of the reactivity of iron zeolites, which were prepared by the three above-noted methods. The results will help to draw conclusions about the reactivity of the iron sites obtained by the different preparation methods.

2. Experimental

2.1. Catalyst preparation

The parent ZSM-5 was obtained from Südchemie (MFI P-46). The sample was partly in the H- and partly in the Na-form. For the chemical vapor deposition of $FeCl_3$; the sample was converted to the H form by 3-fold exchange with a 1 M NH_4NO_3 solution followed by calcination in O_2 at 773 K. Sublimation of $FeCl_3$, washing, and subsequent calcination in O_2 at 773 K (heating rate 1 K/min) were carried out as described before [16,26]. The calcined material is referred to as Fe-ZSM-5 CVD.

Fe-ZSM-5 HT was synthesized according to a procedure described in the literature [27]. The silicate mixture was prepared by adding tetraethoxysilane (TEOS) to a solution of tetrapropylammonium hydroxide (TPAOH, 20% in water), and pure sodium hydroxide. Separately $Fe(NO_3)_3 \cdot 9H_2O$ and $Al(NO_3)_3 \cdot 9H_2O$ were dissolved in deionized water. The synthesis mixture was obtained by dropwise addition of the silicate mixture to an aqueous solution of the metal ions. The molar ratios were $H_2O/SiO_2 = 45$ (including the water in the TPAOH solution), $TPAOH/SiO_2 = 0.1$, $NaOH/SiO_2 = 0.2$, $SiO_2/Al = 36$, and $SiO_2/Fe = 152$. Hydrothermal synthesis was performed in a Teflon-lined stainless-steel autoclave at 448 K for 5 days. A white powder was obtained, which was filtered and washed with water. Calcination was performed at 823 K in air for 10 h. The calcined material was converted into the H-form by three exchanges with a 0.1 M NH_4NO_3 solution, followed by calcination at 823 K in air for 5 h.

Fe-ZSM-5 IEA was prepared by ion exchange of H/Na-ZSM-5 with $FeCl_2$ in aqueous solution. To avoid oxidation of Fe^{2+} to Fe^{3+}, the suspension was degassed with N_2 before adding the $FeCl_2 \cdot 4H_2O$ salt ($Fe/Al = 0.6$). The system was stirred for 22 h at 323 K. Then the solid was filtered, washed, and calcined in air at 773 K.

Fe-ZSM-12 IEM and Fe-ZSM-5 IEM were prepared by ion exchange in methanol. Dry methanol (400 ml/g zeolite) was degassed with N_2 to remove air, before adding dry H-ZSM-12 [28] and $FeSO_4 \cdot 7H_2O$ ($Fe/Al = 1.2$). The suspension was refluxed at 328 K for 24 h under N_2 atmosphere. Then the solid was filtered, washed with water, and dried. The same method was applied to a ZSM-5 sample. The Fe^{2+} ions used for the ion exchange were readily converted to Fe^{3+} during drying (exposure to air), calcination, or steaming.

Steaming of the materials was performed at a vapor pressure of 300 hPa, a temperature of 873 K (heating rate 10 K/min), for 6 h. Fe-ZSM-12 IEM was steamed directly after drying, without prior calcination.

Table 1
Steady-state activity of the catalysts in N_2O decomposition: 2500 ppm N_2O, balance He, GHSV = 40,000 h^{-1}

Catalyst	Fe%	Fe/Al	k_{N_2O}	E_a (kJ/mol)	TOF (10^{-3} s^{-1})
ZSM-5 CVD	4.0	1.1	3.5	120	1.2
ZSM-5 CVD st			5.3	145	1.6
ZSM-5 IEA	0.8	0.25	2.0	145	3.7
ZSM-5 IEA st			3.0	190	5.6
ZSM-5 HT	1.0	0.35	0.3	182	0.5
ZSM-5 HT st			2.8	190	3.9
ZSM-5 IEM	2.0	0.56	0.3	125	0.2
ZSM-5 IEM st			0.0	n.d.	0.0
ZSM-12 IEM	1.6	0.65	0.4	180	0.4
ZSM-12 IEM st			7.6	190	6.6

k_{N_2O} = first-order rate constant at 723 K, in 10^{-4} mol/(s g_{cat} bar).
E_a was determined in the range of 673 to 773 K.

Elemental analysis was carried out by atomic absorption spectroscopy, after dissolving the samples in HF and 2.5 M HNO_3 (see Table 1). In the following the samples are referred to by the name of the zeolite and the extension CVD, IEA, IEM, or HT for the preparation method. "st" is added to indicate that the sample was steamed.

2.2. Catalyst characterization

Diffuse reflectance UV-Vis spectra of the catalysts were measured on a Cary 400 UV-Vis spectrometer equipped with a Praying Mantis sample stage from Harrick. $BaSO_4$ was used as a reference. IR spectra of the materials were recorded on a Bio-Rad FTS 3000 Excalibur spectrometer. Samples were pressed in self-supported pellets of 3–6 mg and degassed at 673 K in inert gas (Ar or He), in order to remove adsorbed water. The spectra were then recorded in transmission mode at 473 K; 64 to 128 scans were accumulated at a resolution of 4 cm^{-1}. For comparison spectra were normalized to the same sample weight. EXAFS spectra were measured at the Swiss Norwegian Beamline at the ESRF Grenoble. A Si(111) monochromator was used. Harmonics were rejected by a Cr-coated mirror. The Fe-K edge was scanned from 6800 to 8000 eV, with a step-size of 0.3 eV in the edge region and of 1 to 4 eV in the postedge region. Four to eight scans were coadded to obtain reasonable signal to noise ratios. EXAFS analysis was carried out using the IFFEFIT software package [29]. The background function was calculated from $\sim$ 25 to 970 eV after the absorption edge. For comparison, background subtraction was also performed with the XDAP 2.3.3 software package. Both led to similar results. Fitting was performed in R space, with a Hanning window ($\Delta k = 0.4$ Å^{-1}) applied before the forward Fourier transformation. The transformation was done between the first node in k space and $k = 11$–13 Å^{-1} (depending on the quality of the data). The fitting interval in R space was 1.0 to 3.0 Å. A Hanning window with $\Delta R = 0.4$ Å was applied to

cut off low and high R contributions. Fitting was performed with FEFFIT (Artemis), the reference paths were calculated using the FEFF8.1 algorithm [30]. Fe_2O_3 was chosen as reference compound. By fitting the experimental spectrum of Fe_2O_3 with the theoretical backscattering paths, ${S_0}^2$ was set to 0.8 and fixed to this value in all subsequent fits.

2.3. N_2O decomposition

Fifty milligrams of catalyst was placed in a quartz reactor of 4 mm inner diameter and treated in a flow of 10% O_2 in He at 773 K for 1 h. Then the reactor was cooled to 573 K (in a flow of He) and 2500 ppm N_2O in He was fed to the reactor. N_2O decomposition was followed for 30 min at each temperature before increasing the temperature by 25–50 K, up to a maximum of 798 K. The total flow was 50 ml/min NTP, corresponding to GHSV = 40,000 h^{-1}. N_2O, N_2, and O_2 were measured by gas chromatography, using a combination of a Porapak Q 80/100 and a Gaschrom MP-1 column with a switching valve. For evaluation of the activity data, the first order rate constant $k = -\ln(1-x)F/(m_{\text{cat}}p)$, the turnover frequency, $\text{TOF} = kp_{N_2O}/n_{\text{Fe}}$ and the activation energy $E_a = \mathrm{d}(\ln k)/\mathrm{d}(1/T)$ were calculated. x is the conversion, F the total flow rate, p the total pressure, and n_{Fe} the concentration of iron (in mol/g).

In the step-response experiments the catalyst was treated in 10% O_2 in He at 773 K for 1 h, in order to remove adsorbed hydrocarbons, and then kept 1 h more at 773 K in a flow of pure He. The reactor was cooled to 673 K and a step-change to 5000 ppm N_2O was performed. After reaching steady state, the flow was stepped down to pure He. For a few selected catalysts, step-up/step-down cycles N_2O–He(t)–N_2O were carried out where t was stepwise increased from 3 to 30 min. The goal of these experiments was to measure the spontaneous desorption of oxygen atoms from the catalyst, i.e., its autoreduction.

In pulse experiments, the catalyst was pretreated at 773 K with 10% O_2 in He, as above. Then a step from He to 1000 ppm N_2O in He was performed at 673 K. Series of six pulses of 5000 ppm N_2O in He were administered (pulse volume 500 µl) to the working catalyst at an interval of 2 min. Finally a step-down to He was performed and 5 min after the step-down a new series of 15 pulses was given.

In the step and pulse experiments a quadrupole mass spectrometer was used for analyzing the reactor effluent. The mass fragments $m/e = 4$ (He), 28 (N_2 and N_2O), 32 (O_2), and 44 (N_2O) were recorded. The signal of He was used for normalization. The time resolution of the mass spectrometric detection was between 2 and 4 s. In the pulse experiments, the width of the pulses (at half height) was $\sim$ 15 s. The pulses were broadened by axial diffusion in the reactor and the tubings. In the step experiments the response time of the system, i.e., the time needed to reach 95% of the final concentration, was $\sim$ 30 s. The system is therefore not suited for following processes, which occur in the ms range. The flow rate in the step and pulse response experiments was always 25 ml/min NTP. The pressure in the reactor was atmospheric. A fresh catalyst was used for each experiment.

3. Results

3.1. IR spectroscopy and elemental analysis

Fig. 1a compares the FTIR spectra of the parent ZSM-12 and the iron-loaded sample, before and after steaming. Bands at 3610 and 3580 cm^{-1} in the parent sample are attributed to Brønsted-OH groups, which point to the 12-ring channel of ZSM-12 and to the inside the channel wall, respectively [31]. After ion exchange with $FeSO_4$, only the intensity of the former band was reduced. This indicates that only the easily accessible OH groups in the 12-ring channel of ZSM-12 could bind iron. Also the intensity of the band attributed to silanol groups at 3735 cm^{-1} was reduced. The maximum of the band shifted from 3735 to 3730 cm^{-1}. In the difference spectrum (not shown) of the parent and the ion-exchanged ZSM-12 a band at 3740 cm^{-1} was found, indicating that also the external silanol-groups reacted with

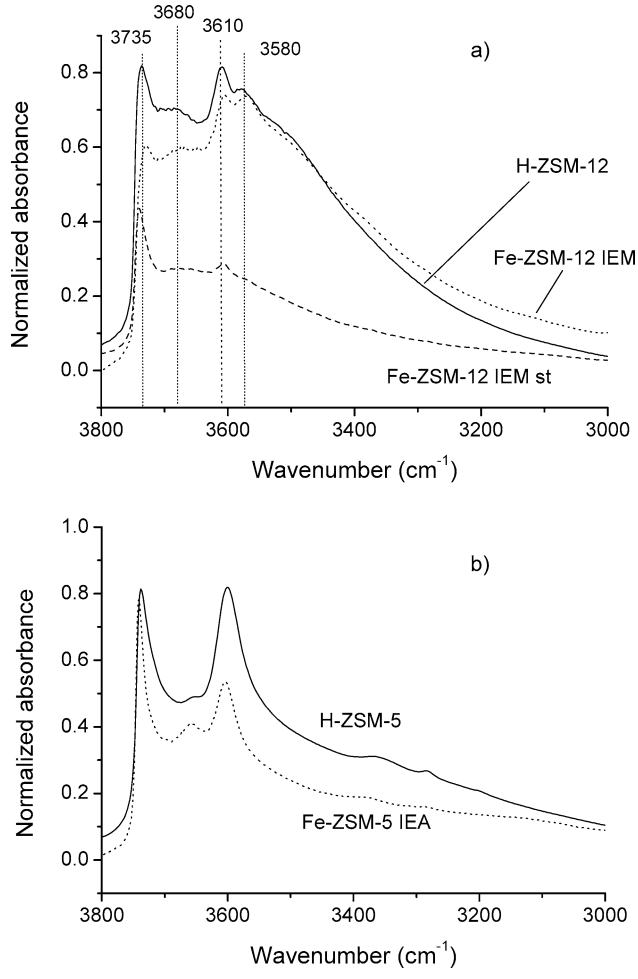

Fig. 1. (a) IR spectra of H-ZSM-12, Fe-ZSM-12 IEM (after ion exchange) and Fe-ZSM-12 IEM st. (b) IR spectra of H-ZSM-5 and Fe-ZSM-5 IEA.

the $FeSO_4$. Elemental analysis showed that the Fe/Al ratio was 0.65 (see Table 1), i.e., more than one Fe^{2+} per two Brønsted acid sites. This is attributed to the above-noted interaction with the silanol groups on the external surface. Steaming of the ion-exchanged sample led to the disappearance of the Brønsted-OH groups inside the channel wall, a large reduction of the concentration of Brønsted-OH groups in the 12-ring channel and an increase of the silanol groups.

In the calcined Fe-ZSM-5 IEA, the intensity of the OH-stretching vibration at 3610 cm^{-1} was reduced to 35% of that of the parent H-ZSM-5 (see Fig. 1b). The band at 3660 cm^{-1}, attributed to extraframework Al–OH, increased compared to the parent sample; the silanol groups did not change. The sample still contained 0.20 wt% Na, corresponding to Na/Al = 0.14. The Fe/Al ratio of the sample was 0.23 (Table 1). The values of Brønsted-OH/Al, Na/Al, and Fe/Al added up to 1.0, showing that one iron atom was bonded to only one ion-exchange site after calcination. The exchange efficiency of $FeCl_2$ was low. Less than half of the iron in the exchange solution was incorporated into ZSM-5.

The IR spectra of Fe-ZSM-5 CVD were reported before [26]. After calcination 60% of the Brønsted acid sites of the parent material remained intact. The concentration of silanol groups did not decrease, showing that the exchange reaction took place exclusively with the Brønsted acid sites. The Fe/Al ratio was 1.1. On average, clusters of 2.8 iron atoms were attached to one Brønsted site.

3.2. UV-Vis spectra

Fig. 2 shows the UV-spectra of Fe-ZSM-5 HT, after hydrothermal synthesis, calcination, and steaming. In the as-synthesized sample two ligand-to-metal charge transfer (LMCT) bands at 41,800 and 46,080 cm^{-1} appeared, as reported before for tetrahedrally coordinated iron atoms in a silicalite framework [32]. A shoulder at 32,500 cm^{-1} was also present. After calcination the shoulder increased in intensity and shifted to higher wavenumbers. Steaming led to a broad, almost featureless UV-Vis spectrum, indicating a strong agglomeration of the iron atoms [33]. A shoulder at 20,000 cm^{-1} indicated the presence of a small concentration of Fe_2O_3 particles [34].

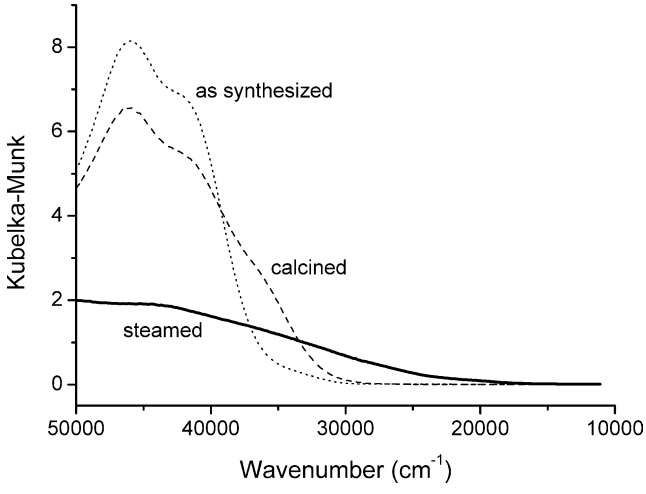

Fig. 2. UV-Vis spectra of Fe-ZSM-5 HT after hydrothermal synthesis, calcination, and steaming.

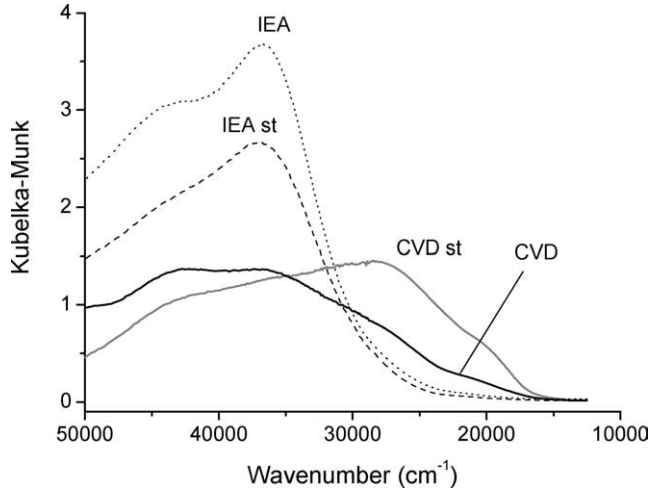

Fig. 3. UV-Vis spectra of Fe-ZSM-5 CVD, CVD st, IEA, and IEA st. The CVD samples were diluted 1:1 with $BaSO_4$.

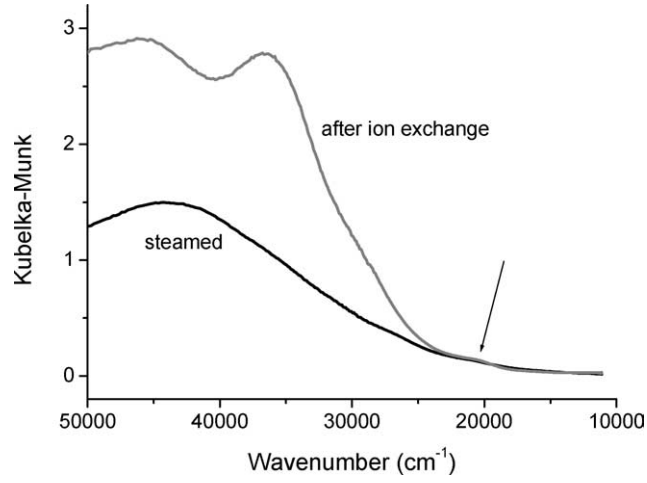

Fig. 4. UV-Vis spectra of Fe-ZSM-5 IEM after ion exchange and subsequent steaming.

The UV-Vis spectrum of Fe-ZSM-5 IEA (Fig. 3) showed two intense charge transfer bands at 44,000 and 36,500 cm^{-1} and only a very weak shoulder at 22,000 cm^{-1}, indicative of Fe_2O_3 clusters. The spectrum is characteristic for isolated iron atoms. Steaming of the catalyst led to a broadening of the LMCT bands, but little agglomeration of the iron clusters was observed.

Fe-ZSM-12 IEM also exhibited very intense LMCT bands (Fig. 4). In comparison to Fe-ZSM-5 IEA, the absorption at 20,500 cm^{-1} was more pronounced, indicating that some large Fe_2O_3 clusters were present next to isolated iron atoms already after the ion exchange. The formation of Fe_2O_3 may be due to the adsorption of $FeSO_4$ on silanol groups on the external surface, which was observed in the

IR spectrum. Steaming led to a broad and featureless UV spectrum, similar to Fe-ZSM-5 HT st.

Fe-ZSM-5 CVD exhibited a stronger absorption below 35,000 cm^{-1} than the two ion-exchanged catalysts (Fig. 3). Absorptions between 35,000 and 25,000 cm^{-1} are characteristic for iron oxo dimers [35]. Moreover, an intense shoulder at 22,000 cm^{-1} was present, which indicates Fe_2O_3 clusters. Steaming increased the absorption between 35,000 and 15,000 cm^{-1}, i.e., it led to strong agglomeration.

3.3. EXAFS

All catalysts exhibited a rather weak EXAFS signal. The spectra were fitted with only one single Fe–O and one single Fe–Fe shell (see Table 2). This two-shell fit enabled a direct comparison of the average Fe–O and Fe–Fe coordination numbers of all the samples. In cases where the data quality allowed the use of a second Fe–O or second Fe–Fe shell, the sum of the Fe–O and Fe–Fe coordination numbers obtained in these fits did not deviate much from the values obtained in the two-shell fit. This assured us that the lumping of all oxygen and iron neighbors into one common backscattering function did not produce erroneous results. The Debye–Waller factors of these lumped shells were very high, however, indicating a large spread of the Fe–O and the Fe–Fe distances, i.e., a high structural disorder. The Fe–O coordination number was between 4 and 5 for all catalysts. The average Fe–O distances were also similar. The Fe–Fe coordination number decreased from Fe-ZSM-12 IEM st and Fe-ZSM-5 HT st (CN $\sim$ 4.0) to Fe-ZSM-5 CVD st (CN $\sim$ 3.5) to Fe-ZSM-5 CVD and Fe-ZSM-5 IEA (CN $\sim$ 2). The steamed catalysts generally had larger Fe–Fe coordination numbers. The coordination number can be seen as a measure for the degree of clustering of the iron atoms.

Table 2
Fit parameters of the EXAFS spectra: R = average distance, CN = coordination number, σ^2 = Debye–Waller factor, ΔE_0 = shift of E_0 compared to the reference

Shell	R (Å)	CN	σ^2 (Å^2)	ΔE_0 (eV)
ZSM-5 CVD				
Fe–O	1.96	4.8 ± 0.5	0.011	−10.5
Fe–Fe	3.01	2.5 ± 1.1	0.014	
ZSM-5 CVD st				
Fe–O	1.98	4.3 ± 0.6	0.011	2.6
Fe–Fe	3.02	3.5 ± 1.2	0.011	
ZSM-5 IEA				
Fe–O	1.99	4.9 ± 1.1	0.012	−7.2
Fe–Fe	3.04	(2.1 ± 3.3)	0.016	
ZSM-5 IEA st				
Fe–O	1.99	5.0 ± 1.3	0.018	−5.8
Fe–Fe	3.06	(3.4 ± 3.5)	0.020	
ZSM-5 HT as				
Fe–O	1.84	2.8 ± 0.8	0.002	−11.4
ZSM-5 HT st				
Fe–O	1.97	4.1 ± 0.6	0.010	−4.6
Fe–Fe	3.03	4.1 ± 2.5	0.017	
ZSM-12 IEM st				
Fe–O	2.02	4.8 ± 0.8	0.009	3.8
Fe–Fe	3.04	3.9 ± 2.0	0.012	

The EXAFS spectrum of the as-synthesized Fe-ZSM-5 HT could be fit with only one Fe–O shell. Its coordination number was 2.8. For iron atoms, which are incorporated into the ZSM-5 framework a value of four would be expected [32]. The discrepancy may be due to the fact that a fraction of the iron species was not in framework positions, but in amorphous clusters with a more distorted coordination. These amorphous clusters might also be responsible for the shoulder at 32,500 cm^{-1}, which was observed in the UV-Vis spectrum. An even lower coordination number (CN = 1.5) was obtained for the calcined sample. Similar results were recently found by Berlier et al. and ascribed to the large heterogeneity of the iron species in the calcined sample [36].

The fit of Fe-ZSM-5 IEA (st) yielded a rather high Fe–Fe coordination number with a large error margin. Choi et al. recently reported an EXAFS analysis of a very similar sample [37] and pointed out that the peak between 2.5 and 3.0 Å in the radial distribution function should be attributed to backscattering by Al and not by Fe. We could fit our spectra equally well with an Al shell, a Fe shell or a combination of both. Due to the narrow k range available for fitting, no firm conclusions could be drawn about the type and number of neighbors in the second coordination shell of iron in these samples.

We also analyzed the preedges of the iron zeolites. Absorption in the preedge is due to a dipole-forbidden 1s $\rightarrow$ 3d transition. Its intensity and position can yield additional information on the oxidation state and coordination geometry of iron [38,39]. The as-synthesized Fe-ZSM-5 HT had a very sharp and intense preedge peak at 7114.5 eV, due to the tetrahedral coordination of the iron atoms in the zeolite framework. All the other samples listed in Table 2 had a less intense preedge peak, also at 7114.5 eV. Differences between the samples could not be detected. None of the preedge peaks had a shoulder at higher energies, which is characteristic for Fe_2O_3 clusters [40]. For all catalysts, the intensity of the peak was higher than that of $Fe(acac)_3$, with octahedral coordination. We can infer that the iron atoms in our catalysts did not have centrosymmetric coordination, but an irregular, distorted coordination sphere.

3.4. Activity in N_2O decomposition

Fig. 5 compares the activity of the catalysts in N_2O decomposition. Fe-ZSM-5 CVD was the most active of the nonsteamed catalysts. Fe-ZSM-5 IEA and Fe-ZSM-12 IEM, which contained mainly isolated iron species, were less efficient in N_2O decomposition. Steaming increased the activity of all catalysts (with one exception). For Fe-ZSM-5 CVD and IEA the effect was small and mainly visible at high

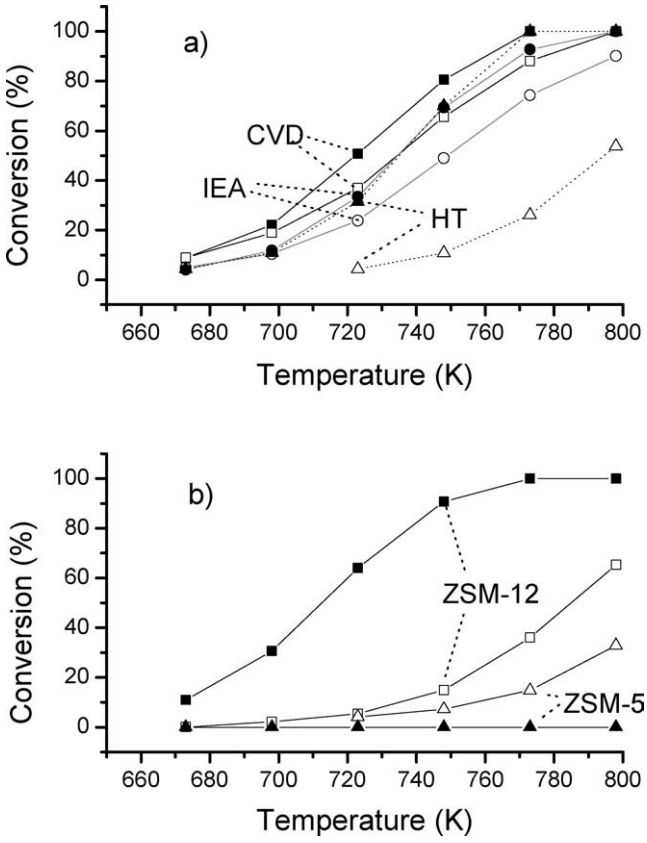

Fig. 5. N_2O decomposition activity. a) Fe-ZSM-5 CVD (squares), IEA (circles) and HT (triangles). b) ZSM-12 IEM (squares) and ZSM-5 IEM (triangles). Steamed samples have full symbols. 2500 ppm N_2O, GHSV = 40,000 h^{-1}.

temperatures. In the case of Fe-ZSM-5 HT and Fe-ZSM-12 IEM, steaming strongly increased the activity. The activation energy of the steamed catalysts was higher (Table 1). In terms of turnover frequency, Fe-ZSM-12 IEM st was the most active catalyst, followed by Fe-ZSM-5 IEA, IEA st, and HT st. Fe-ZSM-5 CVD, and CVD st had a rather low turnover frequency.

The ion exchange with $FeSO_4$ in methanol, followed by steaming led to a very active catalyst in the case of ZSM-12. When the same method was applied to ZSM-5 large Fe_2O_3 clusters were formed, which were almost inactive for N_2O decomposition. The reasons for this very different behavior of the two zeolites are not clear.

3.5. *Step-response experiments*

Step-response experiments were carried out in order to follow the deposition of oxygen from N_2O on the catalyst surface and its subsequent desorption as O_2. This technique was already used to study the N_2O decomposition over Fe-ZSM-5 CVD after pretreatment in oxidative, inert, or reductive atmosphere, at 673 K [41]. The step response of Fe-ZSM-5 CVD shown in Fig. 6 differed strongly from those reported in the previous publication, due to the higher pretreatment temperature used here (773 K). Immediately after

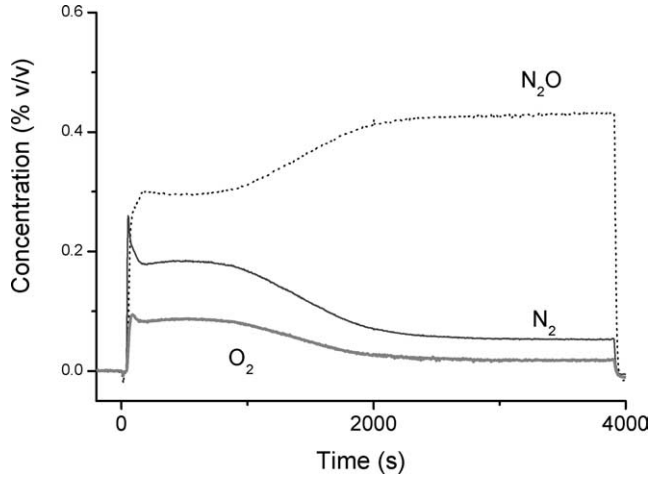

Fig. 6. Step response of Fe-ZSM-5 CVD at 673 K, 5000 ppm N_2O, GHSV = 20,000 h^{-1}.

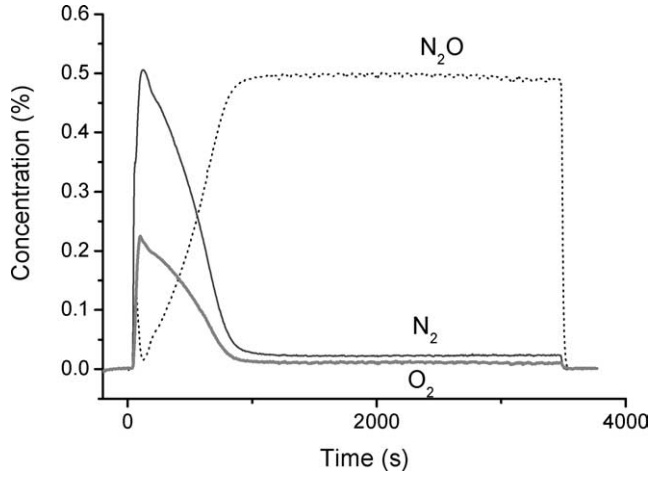

Fig. 7. Step response of Fe-ZSM-5 CVD st at 673 K, 5000 ppm N_2O, GHSV = 20,000 h^{-1}.

the step to N_2O a sharp peak of N_2 was formed, due to reoxidation of Fe^{II} to Fe^{III}. The amount of N_2 formed in this reaction corresponded to 0.02 N_2/Fe, which is significantly more than after pretreatment at 673 K. In that case only 0.01 N_2/Fe was formed. This shows that the pretreatment in inert gas at 773 K led to a higher degree of autoreduction of Fe^{III} to Fe^{II}. The initial, sharp peak of N_2 was followed by a somewhat broader peak of N_2 and O_2 and then by a very broad shoulder of N_2 and O_2, which slowly decayed to steady state [42]. This fast initial N_2O decomposition reaction, which lasted for about 30 min, is called transient N_2O decomposition in the following.

Steaming of the catalyst strongly accelerated the transient reaction (see Fig. 7). A very high initial N_2O decomposition activity was observed, which rapidly decayed to steady state. Qualitatively, the step response showed the same features as for the unsteamed material: an initial peak of N_2 (only visible as a shoulder) produced by the reoxidation of Fe^{II} sites, a peak of N_2 and O_2, and then the broad feature of the transient reaction.

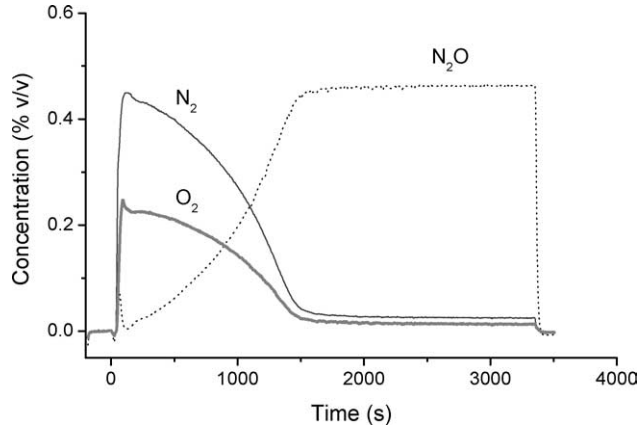

Fig. 8. Step response of Fe-ZSM-5 HT st at 673 K, 5000 ppm N_2O, GHSV = 20,000 h^{-1}.

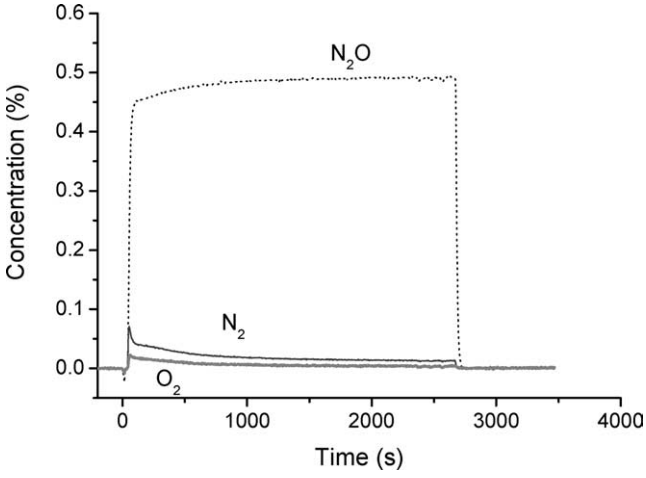

Fig. 9. Step response of Fe-ZSM-12 IEM at 673 K, 5000 ppm N_2O, GHSV = 20,000 h^{-1}.

Fe-ZSM-5 HT st exhibited a similar step response, with a high initial N_2O decomposition activity (Fig. 8). Fe-ZSM-5 IEA and Fe-ZSM-12 IEM showed no or very little transient activity. The catalysts reached steady state immediately after the reoxidation of Fe^{II} sites. In both cases, steaming led to a drastic increase of the transient activity. The effect of steaming was particularly pronounced for Fe-ZSM-12 IEM, as can be seen by a comparison of Figs. 9 and 10. With Fe-ZSM-12 IEM st, transient activity lasted for more than half an hour, before steady state was finally reached. Table 3 compares the amount of N_2 produced during the transient reaction. It was especially large for the catalysts Fe-ZSM-5 HT st and Fe-ZSM-12 IEM st. Steaming always increased the rate and extent of the transient reaction. There was no correlation between transient and steady-state activity.

After the step-down from N_2O to pure He, the O_2 concentration always tailed, while the N_2 concentration decreased to zero without delay. This confirms that O_2 desorption was the rate-limiting step for all catalysts. Since O_2 desorption is related to the autoreduction of the catalyst, a correlation between the degree of autoreduction and the reaction rate

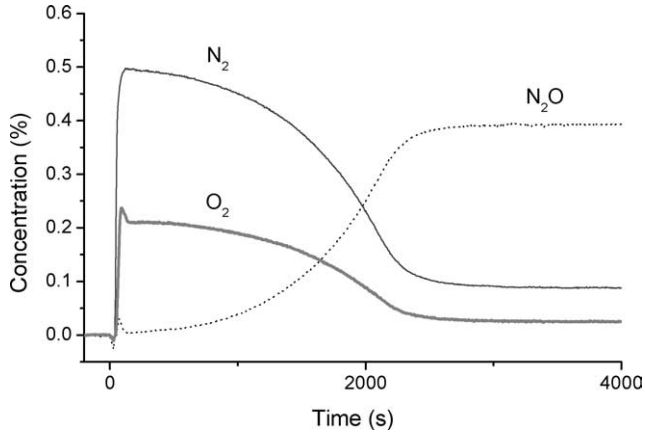

Fig. 10. Step response of Fe-ZSM-12 IEM st at 673 K, 5000 ppm N_2O, GHSV = 20,000 h^{-1}.

Table 3
Step from He to N_2O at 673 K, after pretreatment in O_2 (1 h) and He (1 h) at 773 K

Catalyst	Reoxidation		Transient reaction	
	N_2 (mmol/g)	N_2/Fe	N_2 (mmol/g)	N_2/Fe
ZSM-5 CVD	0.014	0.02	0.70	1.0
ZSM-5 CVD st	0.018	0.02	0.85	1.2
ZSM-5 IEA	0.008	0.05	0.002	0.02
ZSM-5 IEA st	0.013	0.06	0.42	2.0
ZSM-5 HT st	0.015	0.12	1.5	11.7
ZSM-12 IEM	0.003	0.01	0.05	0.2
ZSM-12 IEM st	0.025	0.09	2.7	9.3

Shown is the N_2 produced during the initial reoxidation of Fe^{II} and the N_2 produced during the transient reaction (steady-state activity subtracted).

can be expected [41]. We measured the autoreduction of the catalyst in a stream of He at 673 K using a series of step-up/step-down cycles N_2O–He(t)–N_2O, in which t was varied from 3 to 30 min. The amount of N_2 produced by the reaction $2Fe^{II} + N_2O \rightarrow 2Fe^{III} + N_2$ in each step-up corresponds to the amount of oxygen atoms desorbed from the catalyst. The oxygen desorption is shown as a function of time in Fig. 11. A small amount of oxygen desorbed rather quickly from the catalyst, i.e., within 3 min. Longer desorption times augmented the extent of autoreduction only slightly. The comparison shows that on the steamed catalysts Fe-ZSM-5 HT st and Fe-ZSM-12 IEM st a larger fraction of the iron sites underwent autoreduction than on Fe-ZSM-5 CVD and IEA. If the concentration of oxygen atoms, which quickly desorb from the catalyst surface, determines the catalytic activity a correlation between the extent of autoreduction after 3 min and the yield of N_2 and O_2 should be found. Fig. 12 shows that the correlation between these two parameters is indeed excellent.

3.6. Pulse-response experiments

In order to obtain more information on the mechanism of O_2 desorption pulse experiments were carried out. Pulses

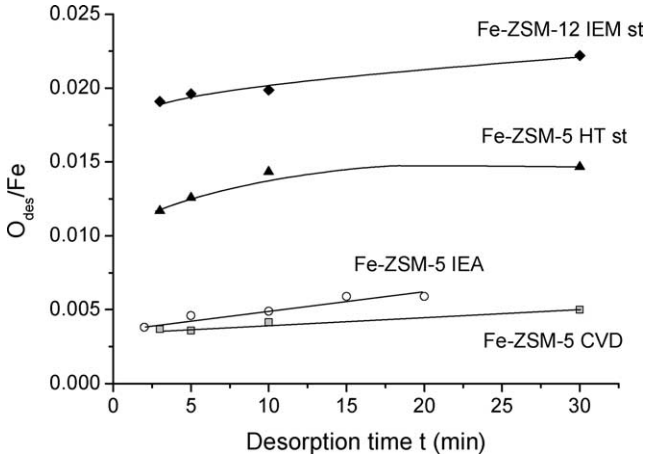

Fig. 11. Oxygen desorption of Fe-ZSM-5 CVD (squares), Fe-ZSM-5 IEA (circles), Fe-ZSM-5 HT st (triangles), and Fe-ZSM-12 IEM st (diamonds) at 673 K in a flow of He, GHSV = 20,000 h^{-1}.

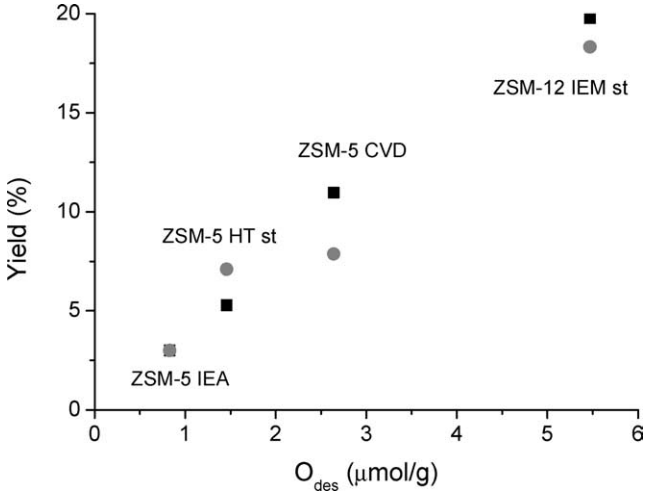

Fig. 12. Relation between the amount of oxygen desorbed from the catalyst in a flow of He at 673 K within 3 min and the steady-state yield of N_2 (squares) and O_2 (circles) in N_2O decomposition at 673 K.

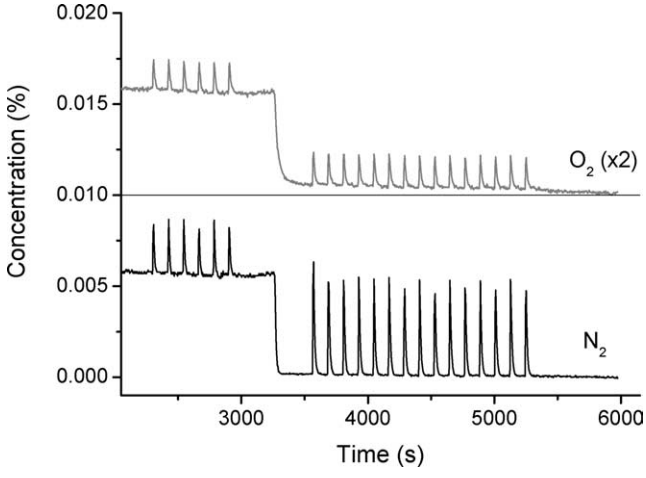

Fig. 13. Pulses of 5000 ppm N_2O during and after N_2O decomposition (1000 ppm N_2O). O_2 is multiplied by 2.0 and offset by 0.01. Fe-ZSM-5 HT at 673 K, GHSV = 20,000 h^{-1}.

Table 4
Left column, oxygen desorbed from the catalyst in a flow of He at 673 K in 3 min; other columns: N_2 and O_2 produced in the pulses of N_2O (5000 ppm) during and after N_2O decomposition at 673 K, GHSV = 20,000 h^{-1}

Catalyst	O_{des} (μmol/g)	During N_2O decomposition		After N_2O decomposition	
		N_2 (μmol/g)	O_2 (×2) (μmol/g)	N_2 (μmol/g)	O_2 (×2) (μmol/g)
ZSM-5 CVD	2.6	0.16	0.15	0.76	0.19
ZSM-5 HT st	1.4	0.09	0.10	0.23	0.10
ZSM-12 IEM st	5.5	0.19	0.13	0.52	0.18
ZSM-5 IEA	0.8	0.07	0.06	0.20	0.06

Accuracy of the values in the pulse experiments is ±0.03 μmol/g.

of N_2O were administered during and after N_2O decomposition. Fig. 13 shows the pulse response of Fe-ZSM-5 HT st. It is qualitatively representative for all other catalysts. Small amounts of N_2 and O_2 were produced in the pulses during steady-state N_2O decomposition. The N_2 peaks were sharper than the O_2 peaks, but, given the accuracy of the measurement, the ratio of the total peak areas did not deviate significantly from the 2:1 stoichiometry of N_2O decomposition (see Table 4). The conversion of N_2O in the pulses was a bit lower than the steady-state conversion. This can be understood from the kinetics of N_2O decomposition. A variation of the partial pressure showed that the order of N_2O in the reaction was ~ 0.7; i.e., a lower N_2O conversion could be expected during the pulses ($c_{N_2O} = 5000$ ppm) than during steady state ($c_{N_2O} = 1000$ ppm).

In the pulses after the step-down to He approximately the same amount of O_2 was produced as in the pulses during the steady-state reaction. The N_2 peaks, however, were larger than during steady state. Especially in the first pulses after the step-down large amounts of N_2 were formed. After a few pulses the N_2 production stabilized at a value that was still two to four times higher than the O_2 production (see Table 4). The 2:1 stoichiometry of the reaction is already accounted for in this comparison. The deposited oxygen atoms, which correspond to excess of N_2 formed in each pulse, were not accumulated on the surface, but desorbed in a continuous process from the catalyst. This can be seen from the gradual drop of the O_2 level as soon as the pulsing was stopped (Fig. 13).

The amounts of N_2 and O_2 produced in the pulses during and after steady-state N_2O decomposition over four different catalysts are compiled in Table 4. The N_2 and O_2 formation in the pulses after the step to He should be related to the concentration of oxygen vacancies on the surface, i.e., to the degree of autoreduction. The amount of N_2/O_2 produced over the different catalysts did indeed follow the same ranking as the concentration of vacancies determined in the step-up/step-down cycles (first column in Table 4). Only Fe-ZSM-12 IEM st was an exception to this rule. Its reactivity in the pulses was low compared to its steady-state reactivity. This will be commented later.

4. Discussion

4.1. Catalyst characterization

The UV spectrum of Fe-ZSM-5 HT is typical of isolated iron ions (Fig. 2). It is dominated by two very intense LMCT bands. Hardly any absorbance is found in the region of the spin-forbidden d–d transitions. The lowest energy LMCT transitions are found at approximately 35,000 cm^{-1} [43]. Strong absorptions below that energy are caused by magnetic coupling of the iron atoms via the superexchange mechanism. Therefore the increase of absorption below 35,000 cm^{-1} is a qualitative measure for the degree of agglomeration of the iron atoms. The UV spectra of Fe-ZSM-5 HT, Fe-ZSM-5 IEA, and Fe-ZSM-12 IEM are dominated by very intense LMCT bands and there is little absorption below 35,000 cm^{-1}. Mainly isolated iron atoms were present in these catalysts. In agreement, the EXAFS spectrum of Fe-ZSM-5 HT could be fit with only one Fe–O shell. No Fe–Fe neighbors were found. Fitting of the Fe-ZSM-5 IEA spectrum led to a Fe–Fe coordination number of two, but the confidence level of that value was low. The information of the UV-Vis spectrum, which shows that the catalyst contains isolated iron atoms, is more trustworthy.

The very broad and featureless bands obtained in the UV-Vis spectra of the steamed samples indicate a large spread of the energy levels of the metal 3d electrons, i.e., highly distorted and inhomogeneous iron clusters. Moreover, the strong absorptions at low energies show that agglomeration of the iron species took place [44]. The EXAFS results confirmed this. The steamed samples had high average Fe–Fe coordination numbers. For ZSM-5 CVD the Fe–Fe coordination number increased from 2.5 to 3.5 upon steaming. Only in the case of Fe-ZSM-5 IEA steaming did not lead to a strong agglomeration.

The fitting of the EXAFS of Fe-ZSM-5 CVD deserves an additional remark: A Fe–Fe coordination number of 1.0 was reported before for this sample, using a fit with three Fe–O and one Fe–Fe shells [26,34]. With the 2-shell fit used here, higher coordination numbers were obtained. These higher coordination numbers are consistent with the clustering observed in the UV-Vis spectra and also with recent Mössbauer data, which indicate that the clustering of the iron atoms in ZSM-5 CVD is higher than originally believed [45].

The results of UV-Vis and EXAFS spectroscopy can be summed up as follows: Ion exchange in aqueous or methanolic solution under careful exclusion of air led to the formation of mainly isolated iron ions bound at the ion-exchange positions. In chemical vapor deposition of $FeCl_3$, small iron oxide clusters with the size of a few atoms were formed. With the exception of Fe-ZSM-5 IEA, steaming led to an agglomeration of the iron clusters and the formation of ill-defined heterogeneous structures, with very broad, featureless UV-Vis spectra.

4.2. The effect of steaming on catalyst activity and the transient reaction

Steaming increased the N_2O decomposition activity of all catalysts. For ZSM-5 samples where iron is incorporated into the zeolite lattice during hydrothermal synthesis the positive effect of steaming is well known [2,46]. In the zeolite framework the iron atoms have no open coordination sites and they are catalytically inactive. Steaming extracts them from the zeolite framework and transforms them to active iron oxide clusters or isolated ions in extraframework positions. It was proposed that these extraframework iron species are bound at ion-exchange positions to framework aluminum and thereby stabilized [47,48].

In ion-exchanged samples the iron atoms are already bound as isolated ions or small clusters at the ion-exchange positions. Steaming is not required to move them there. Yet, we observed a positive effect of steaming also for the iron catalysts prepared by ion exchange in the liquid or the gas phase. Zhu et al. also reported an increased N_2O decomposition activity of their Fe-ZSM-5 CVD catalyst after calcination or steaming at 973 K [49]. The increase in activity was ascribed to the formation of FeO^+ cations from Fe_xO_y clusters during the high-temperature treatment. Very recently, another model was proposed to explain the increased activity of the iron zeolites after high-temperature treatments, namely the formation of Fe–O–Al adducts [50]. This proposal would be in line with our observation that the effect of steaming was especially strong for the ZSM-12 sample, which is more prone to dealumination than ZSM-5 [51].

Steaming had a second, very marked effect on the behavior of the catalysts: The so-called transient reaction drastically increased after the steam treatment. The increase was more pronounced for the samples prepared by ion exchange in the liquid phase, i.e., Fe-ZSM-5 IEA and Fe-ZSM-12 IEM, than for Fe-ZSM-5 CVD. The latter sample already showed a considerable transient activity before steaming. Note that Fe-ZSM-5 CVD exhibited transient activity only after pretreatment at 773 K, but not at 673 K [41]. This indicates that the transient reaction can be activated either by steaming and/or by a pretreatment of the samples at high temperatures in inert gas. The onset of the transient reaction was always slightly delayed. This can be seen from the fact that the N_2O concentration started to rise initially, reached a maximum and then decreased again as soon as the transient reaction started (see Figs. 6–10). The onset of the transient reaction was always preceded by the reoxidation of Fe^{II}-sites. This suggests that the oxygen atoms, which were deposited during reoxidation, catalyze the transient reaction, e.g., via an Eley–Rideal-type scavenging of the deposited oxygen atoms by N_2O:

$$*\text{–}O + N_2O \rightarrow N_2 + O_2.$$

The large amount of N_2 and O_2 produced in the transient reaction (N_2/Fe is larger than 0.5 for some of the catalysts) shows, however, that the reaction is a catalytic cycle and not

only a one-time scavenging of the oxygen atoms deposited during reoxidation. An explanation why the reaction deactivates and decays to steady state cannot be given here. Since there was no correlation between the extent of the transient reaction and the steady-state activity, the occurrence of the transient reaction cannot explain the increased steady-state activity of the samples after steaming.

4.3. The relation between activity and O_2 desorption

O_2 desorption is the rate-limiting step of N_2O decomposition [52]. It was recently shown that, for a series of iron zeolites prepared by chemical vapor deposition, a correlation between the rate of N_2O decomposition and the autoreduction of the catalyst exists [41]. Autoreduction is associated with the creation of oxygen vacancies by spontaneous O_2 desorption from the catalyst. The data presented here show that the correlation between autoreduction at 673 K and the activity of the catalyst is valid for a large range of iron zeolites prepared by different methods (Fig. 12).

In the step response experiments (Table 3 and Figs. 6–10) the catalysts were pretreated for 1 h at 773 K before the step to N_2O. Therefore, the peak of N_2, which was produced right after the step by reoxidation of Fe^{II}, corresponds to the autoreduction at 773 K. Autoreduction at 773 K (Table 3) was significantly higher than at 673 K (Table 4). On Fe-ZSM-5 HT st and Fe-ZSM-12 IEM st 20–25% of the iron sites underwent autoreduction, on the other catalysts it was less than 10%. We compared the absolute extent of autoreduction at 773 K with the steady-state activity of the catalysts at 748 K. At 773 K most catalysts obtained 100% conversion and the values were not suited for comparison. The good correlation shown in Fig. 14 proves that the ease of O_2 desorption from the catalyst also governs the activity at high reaction temperatures.

The pulse experiments show more details about the mechanism of O_2 desorption. When pulses of a higher concentration of N_2O were administered to the catalyst during steady-state N_2O decomposition, peaks of N_2 and O_2 were formed. The O_2 peaks were broader and slightly delayed with respect to N_2, but the O_2 formation was not entirely smeared out in the continuous O_2 desorption process. Interestingly, the same amount of O_2 was released from the surface in the pulses after the step back to pure He. During these pulses the concentration of vacancies was higher than during the steady-state reaction and more N_2O molecules could deposit oxygen atoms on the catalyst surface, as indicated by the higher N_2 formation. Yet, only the same amount of O_2 as during the steady-state reaction could desorb in a relatively sharp peak whereas the rest was released in a slow, continuous process. This shows that the fast O_2-desorption process is not limited by the availability of deposited oxygen atoms, but by the concentration of active sites, which enable a quick recombination to O_2. If there is an excess of deposited oxygen atoms, as in the pulses after N_2O decomposition, then they are gradually desorbed from other iron centers, which allow only a rather slow recombination of oxygen atoms. There is reason to believe that fast and slow O_2-desorption process contributes to the steady-state activity: (i) The increased activity of Fe-ZSM-5 CVD after reductive pretreatment [41] can be understood in that picture. During the reoxidation of a reduced catalyst with N_2O, a large amount of N_2O-oxygen atoms is deposited on its surface. Above we showed that a high concentration of deposited oxygen atoms does not accelerate the fast O_2 desorption process because it is limited by the availability of active sites. Therefore, the N_2O-oxygen atoms deposited on a reduced catalyst can only increase the reaction rate by incrementing the contribution of the slow O_2 desorption process to the overall activity. (ii) For Fe-ZSM-12 IEM st a comparatively small amount of O_2 was released during the pulses (Table 4), although the catalyst had a very high steady-state activity. This indicates that the slow O_2-desorption process contributed a great deal to the total activity. The observation that a large drop of the O_2 level was observed on Fe-ZSM-12 IEM st as soon as the N_2O pulses were stopped is consistent with that idea. The drop of the oxygen level after the N_2O pulses can be used as a rough measure for the extent of the slow O_2-desorption process. It decreased in the order Fe-ZSM-12 IEM st $\sim$ Fe-ZSM-5 CVD > Fe-ZSM-5 HT st > Fe-ZSM-5 IEA. A small drop was observed for the catalysts with low iron loadings, a large drop for the catalysts with high iron loadings and a high degree of agglomeration. This suggests that the slow oxygen desorption process is associated with a migration of the oxygen atoms on the catalyst surface, which is facilitated by high iron loadings.

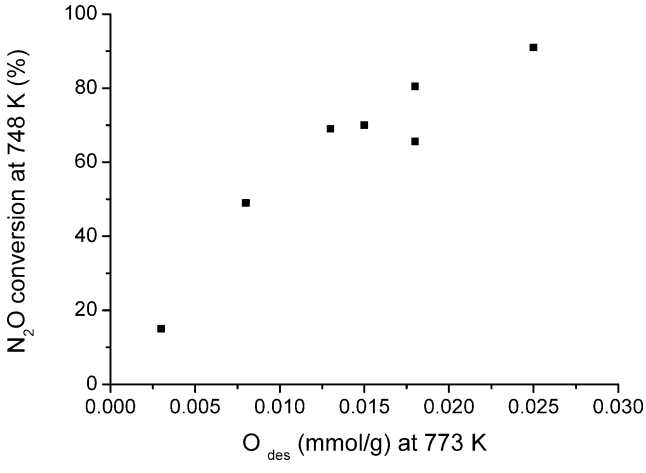

Fig. 14. Steady-state N_2O conversion at 748 K (2500 ppm N_2O, GHSV = 40,000 h^{-1}) vs the concentration of oxygen atoms desorbed from the catalyst at 773 K during 1 h in He-flow (GHSV = 20,000 h^{-1}).

Fast and slow oxygen desorption could be distinguished as Eley–Rideal and Langmuir–Hinshelwood-type reactions. However, the TAP experiments by Mul et al. [52] and our own isotope-labeling experiments [53] speak against the involvement of an Eley–Rideal mechanism. We therefore prefer to assign the fast oxygen desorption to the recombination of two oxygen atoms which were deposited in close vicinity

to each other whereas the slow oxygen desorption is preceded by exchange and migration of the oxygen atoms over the whole iron oxide cluster.

4.4. The relation between structure and activity

The dominating iron species in Fe-ZSM-5 IEA, Fe-ZSM-5 CVD, Fe-ZSM-5 HT st and Fe-ZSM-12 IEM st are, according to the characterization data, isolated iron centers (ZSM-5 IEA), iron oxide clusters of 2–4 iron atoms (ZSM-5 CVD) and unspecified, probably larger iron oxide clusters in the steamed samples. Despite the different iron species present in the catalysts, their activity is governed by the same autoreduction curve (Fig. 12). Also their response to the pulses of N_2O was qualitatively similar. Steaming increased the activity of all catalysts and generated the so-called transient reaction. All these observations indicate that there is no fundamental difference between the catalytic behavior of the different iron zeolites. Only the contribution of fast and slow O_2-desorption process seems to distinguish the iron species. This agrees with the recently expressed opinion [54] that, with the exception of very large Fe_2O_3 clusters, all iron sites contribute to catalytic activity, to a smaller or larger extent.

In principle, another explanation can be given for the similar behavior of all iron zeolites, which is diametrically opposed to the hypothesis discussed above: the same active iron species might be present in all the samples, but in a very low concentration so that it escapes detection by averaging characterization methods. Recent isotope-labeling experiments showed that oxygen desorption is preceded by a fast scrambling of the surface oxygen atoms [53]. The size of the oxygen pool, which takes part in the exchange reaction is large: $O_{pool}/Fe \sim 1$ for Fe-ZSM-5 CVD. From this we infer that all (or most of) the iron atoms are involved in O_2 desorption and cannot be regarded as mere spectators in the reaction. Different iron species may, however, contribute to a different extent and also in a different way to the total activity. In the pulse experiments we could distinguish a fast and a slow O_2 desorption process. The slow O_2 desorption process had a very small contribution on Fe-ZSM-5 IEA and relatively large one on Fe-ZSM-5 CVD. Consequently, the TOF of Fe-ZSM-5 IEA was high and the TOF of Fe-ZSM-5 CVD low. This indicates that the intrinsic activity of isolated iron species is higher. The highest TOFs were, however, observed for the steamed samples, which mainly contained rather large iron clusters (with the exception of Fe-ZSM-5 IEA st). Such iron oligomers were designated by Perez-Ramirez et al. as the main active sites in N_2O decomposition over Fe-ZSM-5 HT st samples [48], but if our argumentation above is correct, these oligomers should have a large contribution of the slow O_2-desorption process and a low TOF. This does not agree with our observations. The very high activation energies of the steamed samples and the occurrence of the transient reaction suggest that steaming brings about a qualitative change in the nature of the iron clusters, instead of simply changing their size. New iron species seem to be formed, which have a higher intrinsic activity. The formation of Fe–O–Al adducts, which was recently proposed by Hensen et al. [50], can explain our experimental observations, but is still open for debate.

5. Conclusions

Different preparation methods, i.e., ion exchange in the liquid phase, chemical vapor deposition, or hydrothermal synthesis, lead to different types of iron species, but their catalytic behavior in N_2O decomposition is qualitatively similar. The rate of O_2 desorption is governing the activity of all catalysts. A fast and a slow O_2 desorption process could be distinguished. Both contribute to steady-state activity. Fast desorption takes place on isolated iron species, while slow desorption is favored by high iron loadings. Slow desorption may therefore be related to the migration of oxygen atoms over the iron clusters before their desorption as O_2. Steaming increases the activity of all catalysts. The positive effect of steaming is tentatively attributed to the formation of Fe–O–Al clusters, as recently proposed by Hensen el al. [50]. Steaming also induces the so-called transient reaction: a very high initial activity in N_2O decomposition, which slowly decays to steady state. Extent and rate of this transient reaction are not related to the steady-state activity.

Acknowledgments

We acknowledge the Swiss National Science Foundation for financial support, Prof. Roel Prins for many fruitful discussions and comments on the manuscript, Maria Eugenia von Potieruchin for assistance in the elemental analysis, Dr. Wouter van Beek and Dr. Hermann Emmerich at the Swiss–Norwegian Beamline, and all members of our EXAFS team for help with the XAS measurements.

References

[1] J. Perez-Ramirez, F. Kapteijn, G. Mul, J.A. Moulijn, Appl. Catal. B 35 (2002) 227.
[2] J. Perez-Ramirez, F. Kapteijn, G. Mul, J.A. Moulijn, Chem. Commun. (2001) 693.
[3] F. Kapteijn, J. Rodriguez-Mirasol, J.A. Moulijn, Appl. Catal. B 9 (1996) 25.
[4] G. Centi, S. Perathoner, F. Vanazza, M. Marella, M. Tomaselli, M. Mantegazza, Adv. Environ. Res. 4 (2000) 325.
[5] J.N. Armor, T.A. Braymer, T.S. Farris, Y. Li, F.P. Petrocelli, E.L. Weist, S. Dannan, C.S. Swamy, Appl. Catal. B 7 (1996) 397.
[6] T.W. Dann, K.H. Schulz, M. Mann, M. Collings, Appl. Catal. B 6 (1995) 1.
[7] X.F. Wang, H.C. Zheng, Appl. Catal. B 3 (1993) 55.
[8] J. Oi, A. Obuchi, G.R. Bamwenda, A. Ogata, H. Yagita, S. Kushiyama, K. Mizuno, Appl. Catal. B 12 (1997) 277.
[9] G. Centi, A. Galli, B. Montanari, S. Perathoner, A. Vaccari, Catal. Today 35 (1997) 113.

[10] J. Perez-Ramirez, J. Overeijnder, F. Kapteijn, J.A. Moulijn, Appl. Catal. B 23 (1999) 51.
[11] H.C. Zheng, X.Y. Pang, Appl. Catal. B 13 (1997) 113.
[12] R.Q. Long, R.T. Yang, J. Catal. 188 (1999) 332.
[13] R.Q. Long, R.T. Yang, J. Catal. 201 (2001) 145.
[14] A. Guzmann-Vargas, G. Delahay, B. Coq, Appl. Catal. B 42 (2003) 369.
[15] K. Krishna, G.B.F. Seijger, C.M. van den Bleek, M. Makkee, G. Mul, H.P.A. Calis, Catal. Lett. 86 (2003) 121.
[16] H.Y. Chen, W.M.H. Sachtler, Catal. Lett. 50 (1998) 125.
[17] H.Y. Chen, W.M.H. Sachtler, Catal. Today 42 (1998) 73.
[18] F. Heinrich, C. Schmidt, E. Löffler, M. Menzel, W. Grünert, J. Catal. 212 (2002) 157.
[19] W.N. Delgass, R.L. Garten, M.J. Boudart, J. Phys. Chem. 73 (1969) 2970.
[20] R.M. Cornell, U. Schwertmann, The Iron Oxides: Structure, Properties, Reactions, Occurrence and Uses, VCH, Weinheim, 1996.
[21] H.Y. Chen, W.M.H. Sachtler, Catal. Today 42 (1998) 73.
[22] L.V. Pirutko, O.O. Parenago, E.V. Lunina, A.S. Kharitonov, L.G. Okkel, G.I. Panov, React. Kinet. Catal. Lett. 52 (1994) 275.
[23] G.I. Panov, A.S. Kharitonov, V.I. Sobolev, Appl. Catal. A 98 (1993) 1.
[24] G.I. Panov, V.I. Sobolev, A.S. Kharitonov, J. Mol. Catal. 61 (1990) 85.
[25] I. Sobolev, G.I. Panov, A.S. Kharitonov, V.N. Romannikov, A.M. Volodin, K.G. Ione, J. Catal. 139 (1993) 435.
[26] P. Marturano, L. Drozdova, A. Kogelbauer, R. Prins, J. Catal. 192 (2000) 236.
[27] A. Ribera, I.W.C.E. Arends, S. de Vries, J. Perez-Ramirez, R.A. Sheldon, J. Catal. 195 (2000) 287.
[28] W. Zhang, P.G. Smirniotis, M. Gangoda, R.N. Bose, J. Phys. Chem. B 104 (2000) 4122.
[29] M. Newville, J. Synchrotron Rad. 8 (2001) 322.
[30] A.L. Ankudinov, B. Ravel, J.J. Rehr, S.D. Conradson, Phys. Rev. B 58 (1998) 7565.
[31] B.H. Chiche, R. Dutartre, F. Di Renzo, F. Fajula, A. Katovic, A. Regina, G. Giordano, Catal. Lett. 31 (1995) 359.
[32] S. Bordiga, R. Buzzoni, F. Geobaldo, C. Lamberti, E. Giamello, A. Zecchina, G. Leofanti, G. Petrini, G. Tozzola, G. Vlaic, J. Catal. 158 (1996) 486.
[33] A.M. Ferretti, C. Oliva, L. Forni, G. Berlier, A. Zecchina, C. Lamberti, J. Catal. 208 (2002) 83.
[34] P. Marturano, L. Drozdova, G.D. Pirngruber, A. Kogelbauer, R. Prins, Phys. Chem. Chem. Phys. 3 (2001) 5585.
[35] R.C. Reem, J.M. McCormick, D.E. Richardson, F.J. Devlin, P.J. Stephens, R.L. Musselman, E.I. Solomon, J. Am. Chem. Soc. 111 (1989) 4688.
[36] G. Berlier, G. Spoto, P. Fisicaro, S. Bordiga, A. Zecchina, E. Giamello, C. Lamberti, Microchem. J. 71 (2002) 101.
[37] S.H. Choi, B.R. Wood, J.A. Ryder, A.T. Bell, J. Phys. Chem. B 107 (2003) 11843.
[38] P.E. Petit, F. Farges, M. Wilke, V.A. Sole, J. Synchrotron Rad. 8 (2001) 952.
[39] T.E. Westre, P. Kennepohl, J.G. DeWitt, B. Hedman, K.O. Hodgson, E.I. Solomon, J. Am. Chem. Soc. 119 (1997) 6297.
[40] L.X. Chen, T. Liu, M.C. Thurnauer, R. Csencsits, T. Rajh, J. Phys. Chem. B 106 (2002) 8539.
[41] G.D. Pirngruber, J. Catal. 219 (2003) 456.
[42] Q. Zhu, R.M. van Teeffelen, R.A. van Santen, E.J.M. Hensen, J. Catal. 221 (2004) 575.
[43] D.M. Sherman, Phys. Chem. Miner. 12 (1985) 161.
[44] E.J.M. Hensen, Q. Zhu, M.M.R.M. Hendrix, A.R. Overweg, P.J. Kooyman, M.V. Sychev, R.A. van Santen, J. Catal. 221 (2004) 560.
[45] A.A. Battiston, J.H. Bitter, F.M.F. de Groot, A.R. Overweg, O. Stephan, J.A. van Bokhoven, P.J. Kooyman, C. van der Spek, G. Vanko, D.C. Koningsberger, J. Catal. 213 (2003) 251.
[46] K.A. Dubkov, N.S. Ovanesyan, A.A. Shteinman, E.V. Starokon, G.I. Panov, J. Catal. 207 (2002) 341.
[47] G. Berlier, A. Zecchina, G. Spoto, G. Ricchiardi, S. Bordiga, C. Lamberti, J. Catal. 215 (2003) 264.
[48] J. Perez-Ramirez, F. Kapteijn, J.C. Groen, A. Domenech, G. Mul, J.A. Moulijn, J. Catal. 214 (2003) 33.
[49] Q. Zhu, B.L. Mojet, R.A.J. Janssen, E.J.M. Hensen, J. van Grondelle, P.C.M.M. Magusin, R.A. van Santen, Catal. Lett. 81 (2002) 205.
[50] E.J.M. Hensen, Q. Zhu, R.A. van Santen, J. Catal. 220 (2003) 260.
[51] J. Cejka, G. Kosova, N. Zilkova, I. Hruba, Stud. Surf. Sci. Catal. 142 (2002) 247.
[52] G. Mul, J. Perez-Ramirez, F. Kapteijn, J.A. Moulijn, Catal. Lett. 77 (2001) 7.
[53] G.D. Pirngruber, P.K. Roy, Catal. Lett. 93 (2004) 75.
[54] J. Perez-Ramirez, F. Kapteijn, A. Brückner, J. Catal. 218 (2003) 234.